ELSEVIER

Applied Catalysis A: General 172 (1998) 333–349

APPLIED CATALYSIS A: GENERAL

Evaluation of the role played by praseodymium molybdates in Pr_6O_{11}–MoO_3 catalysts for the selective oxidation of isobutene to methacrolein

F. De Smet[a], P. Ruiz[b], B. Delmon[b], M. Devillers[a,*]

[a]*Université Catholique de Louvain, Laboratoire de Chimie Inorganique et Analytique, Place Louis Pasteur, 1, B-1348 Louvain-la-Neuve, Belgium*

[b]*Université Catholique de Louvain, Unité de Catalyse et de Chimie des Matériaux Divisés, Place Croix du Sud, 2, B-1348 Louvain-la-Neuve, Belgium*

Received 24 February 1998; received in revised form 16 April 1998; accepted 16 April 1998

Abstract

The catalytic role played by praseodymium molybdate phases (Pr_6MoO_{12}, Pr_2MoO_6, $Pr_2Mo_3O_{12}$) generated in Pr_6O_{11}–MoO_3 catalysts during their use in the selective oxidation of isobutene to methacrolein is evaluated in order to determine whether the observed synergetic effects have to be assigned to cooperation between binary praseodymium and molybdenum oxides, or to the occurrence of praseodymium molybdate phases, that would be catalytically active themselves or would act synergetically with MoO_3 or Pr_6O_{11}. X-ray diffraction, infrared spectroscopy, X-ray photoelectron spectroscopy and time-of-flight secondary ion mass spectrometry (ToF SIMS) are used to determine the composition of the used Pr_6O_{11}–MoO_3 catalysts. Pr_6MoO_{12} appears to be the major ternary phase present in the bulk and $Pr_2Mo_3O_{12}$ is predominant at the surface. To understand the catalytic behaviour of the Pr_6O_{11}–MoO_3 mixtures, the catalytic performances of the pure praseodymium molybdate phases and those of their mixtures with MoO_3, Sb_2O_4 and Pr_6O_{11} were also examined. It is shown that the cooperative effects previously observed in the MoO_3–Pr_6O_{11} mixtures most probably cannot be assigned exclusively to the intrinsic catalytic properties of praseodymium molybdates. A cooperation is also observed between other couples of oxide phases, i.e. Pr_6MoO_{12} displays donor properties with respect to MoO_3. It appears also that the evolution of the catalytic properties of Pr_6MoO_{12}–MoO_3 mixtures with respect to the Pr/Mo content is completely different from the one observed in MoO_3–Pr_6O_{11} mixtures. In addition, it does not seem that the observed synergetic effects could be assigned to the simultaneous presence of ternary $Pr_xMo_yO_z$ phases and Pr_6O_{11}. The generation of praseodymium molybdate phases during the catalytic tests seems therefore to play no significant role in the catalytic behaviour of MoO_3–Pr_6O_{11} mixtures.

Keywords: Molybdate; Praseodymium; Selective oxidation; Synergy

1. Introduction

During the last few years, the catalytic performances of multiphasic oxide-based catalysts were

*Corresponding author. Tel.: 0032 10-472 827; fax: 0032 10-472 330; e-mail: devillers@inan.ucl.ac.be

0926-860X/98/$19.00
PII S0926-860X(98)00130-6

analysed within the framework of the ''remote control'' theory, based on the migration of active oxygen species (''spill-over'' oxygen) from a donor to an acceptor phase. The central feature of this mechanism is that a cooperation occurs between two oxide phases. The first one, called the acceptor, is the catalytically active phase for the oxidation reaction, while the second one, called the donor, shows no intrinsic catalytic behaviour, but governs the efficiency of the first one by creating and/or regenerating selective active sites on its surface. This mechanistic model has been successful in accounting for the synergetic effects observed on the yield and selectivity of a wide range of multiphasic oxidation catalysts [1–5]. To help understand the overall behaviour of lanthanide elements in oxidation catalysis, it seemed therefore interesting to investigate whether their oxides give rise to cooperation effects in the selective oxidation of isobutene to methacrolein, and whether these effects can be rationalized within the above-mentioned model.

In a previous work [6], the behaviour of five lanthanide oxides (La_2O_3, Sm_2O_3, CeO_2, Pr_6O_{11}, Tb_4O_7) with respect to the selective oxidation of isobutene to methacrolein was investigated as pure phases but also during experiments in which these oxides were mixed mechanically with either Sb_2O_4 (oxygen donor) or MoO_3 (oxygen acceptor). Among the five lanthanide oxides tested, only CeO_2 and Pr_6O_{11} were found to give rise to pronounced cooperation effects when mixed with MoO_3.

The behaviour of cerium oxide could be interpreted rather easily because cooperation effects occurred without apparent formation of new phases during the catalytic tests. CeO_2 was consequently identified as potential donor phase of spill-over oxygen.

In the case of praseodymium oxide, the interpretation of the experimental data was much less straightforward. In the Pr_6O_{11}–MoO_3 mechanical mixtures, increasing amounts of Pr_6O_{11} were found to cause a decrease in the conversion rate of isobutene, with an apparent minimum in the Pr_6O_{11}-rich composition range. In the same sample series, positive synergetic effects appeared essentially on the methacrolein yield, which reached a maximum for the same composition as above. These conclusions remained valid when considering the intrinsic yields, confirming that the observed effects could not be assigned to changes in the specific surface area. In most cases, when positive synergetic effects were noted on the yield in the partial oxidation product, a simultaneous decrease of total oxidation was observed. X-ray diffraction measurements performed on the used catalysts showed that praseodymium molybdate phases (Pr_6MoO_{12}, Pr_2MoO_6, $Pr_2Mo_3O_{12}$) were formed in situ under the reaction conditions. All the Sb_2O_4–Pr_6O_{11} mechanical mixtures gave rise to a positive synergy on the methacrolein production. In Sb_2O_4-rich mixtures, the overall isobutene conversion was decreased and CO_2 production was completely inhibited.

Owing to the appearance of praseodymium molybdate phases in Pr_6O_{11}–MoO_3 catalysts under the reaction conditions, additional experiments were undertaken to look whether the catalytic behaviour could be rationalized within the framework of the remote control theory.

The purpose of the present work is therefore (i) to identify more accurately the praseodymium molybdate phases (Pr_6MoO_{12}, Pr_2MoO_6, $Pr_2Mo_3O_{12}$) generated, (ii) to determine their stability under the reaction conditions, (iii) to measure their intrinsic catalytic performances in isobutene oxidation, and (iv) to evaluate their behaviour within the framework of the remote control theory. The keypoint remains to determine whether the observed synergetic effects in Pr_6O_{11}–MoO_3 catalysts have to be assigned to cooperation between praseodymium and molybdenum oxides, or to the occurrence of these praseodymium molybdate phases, namely whether they are catalytically active themselves and/or act synergetically with MoO_3 or Pr_6O_{11}.

The strategy adopted to answer these questions was based on the following experimental steps. The pure praseodymium molybdate phases were synthesized by the citrate route. Mechanical mixtures of various compositions between the molybdates $Pr_xMo_yO_z$ and MoO_3 (typical acceptor), Sb_2O_4 (typical donor) or Pr_6O_{11} were prepared. The catalytic performances of the pure $Pr_xMo_yO_z$ phases and the previously described mixtures were measured in the partial oxidation of isobutene to methacrolein at 673 K. The catalytic behaviour of the pure $Pr_xMo_yO_z$ phases and MoO_3–Pr_6O_{11} mixtures having the same molar composition as the three praseodymium molybdate phases were compared, and also those of MoO_3–Pr_6O_{11} mixtures and Pr_6MoO_{12}–MoO_3 mixtures

having the same Pr/Mo molar ratio. The fresh and used catalysts were studied by X-ray diffractometry (XRD), FT-IR spectroscopy and X-ray photoelectron spectroscopy (XPS) in order to characterize the phases generated by solid state reactions during the catalytic process. Additional information on the surface composition of these catalysts was also obtained using secondary ion mass spectrometry (SIMS) in the time-of-flight (ToF) mode and has been published elsewhere [7].

2. Experimental

2.1. Catalysts preparation

2.1.1. Pure oxides

Praseodymium(III,IV) oxide, Pr_6O_{11}, was purchased from Janssen Chimica (99.9%). MoO_3 was obtained by calcination of a citrate-type complex [8] at 673 K for 20 h. The citrate precursor was synthesized from solutions of ammonium heptamolybdate (Merck, 99%; 0.2 mol l^{-1}) and citric acid (Merck, 99.6%; 1.6 mol l^{-1}); the gel obtained after partial elimination of water was subsequently heated under vacuum at 363 K for 20 h, and then, after grinding, at 573 K in air for a further 20 h period. α-Sb_2O_4 was prepared by calcination of Sb_2O_3 (Merck, >99%) in air at 773 K for 20 h.

2.1.2. Praseodymium molybdates

Three praseodymium molybdate phases, Pr_6MoO_{12}, Pr_2MoO_6 and $Pr_2Mo_3O_{12}$, were also obtained by calcination of citrate-type complexes. The precursors were synthesized from solutions containing amounts of ammonium heptamolybdate and praseodymium(III) nitrate hexahydrate (Aldrich, 99.9%) corresponding to the stoichiometry of the wanted $Pr_xMo_yO_z$ phase, in the presence of citric acid. The gel obtained after partial removal of water was subsequently heated under vacuum at 363 K for 20 h, and then, after grinding, at 1073 K in air for a further 20 h period.

2.1.3. Mechanical mixtures

The mechanical mixtures were obtained by dispersing the adequate amount of the concerned oxides under ultrasonic stirring in 100 ml distilled *n*-heptane during 15 min. The hydrocarbon was then slowly eliminated (in about 1 h) up to dryness under reduced pressure, at room temperature. This procedure was selected in order to minimize, as far as possible, any damage to the crystallites during the mixing procedure, as would actually be expected to occur more easily upon dry grinding in a mortar. It was also shown to provide better homogeneity than the latter. The catalysts were used in the catalytic tests without any further thermal treatment. These catalysts are characterized by their weight ratio (x_m) defined as the ratio of the mass of lanthanide oxide or molybdate phase to the total mass of the mixture.

2.2. Analytical techniques

2.2.1. X-ray diffractometry (XRD)

Powder X-ray diffraction spectra were measured on a Kristalloflex Siemens D5000 diffractometer using the copper K_α radiation (λ=154.18 pm). The samples were analysed after deposition on a quartz monocrystal sample-holder supplied by Siemens. The crystalline phases were identified by reference to the powder diffraction data (JCPDS-ICDD).

2.2.2. Infrared spectroscopy (IR)

Infrared spectra were registered on a Perkin-Elmer type 1710 Fourier transform spectrometer. Samples were analysed in the form of KBr disks (90 wt% KBr) pelletized under a pressure of 8 tons cm^{-2}. Spectra were recorded with background correction in the wave number range 1000–400 cm^{-1}.

2.2.3. X-ray photoelectron spectroscopy (XPS)

X-ray photoelectron spectroscopy was performed on an SSI-X probe (SSX-100/206) spectrometer from FISONS, using the Al-K_α radiation (E=1486.6 eV). The energy scale was calibrated by taking the Au $4f_{7/2}$ binding energy at 84 eV. The C_{1s} binding energy of contamination carbon set at 284.8 eV was used as internal standard value. The analysis of molybdenum and praseodymium were based on the Mo 3d and Pr $3d_{5/2}$ photopeaks (cf. Table 1).

2.2.4. Specific surface area measurements (BET)

The BET specific surface area measurements were carried out on a Micromeritics ASAP 2000 analyser, using krypton at 77 K. Samples were previously outgassed under vacuum at 423 K.

Table 1
XPS results

Sample	x_m[a]	Pr/Mo molar ratio		
		Theoretical	Experimental	
			Fresh	Used
Pr_6MoO_{12}	—	6.0	6.5	—
$Pr_2Mo_3O_{12}$	—	0.7	1.0	—
Pr_2MoO_6	—	2.0	2.2	—
Pr_6O_{11}–MoO_3	0.5	0.8	0.9	0.3
Pr_6O_{11}–MoO_3	0.75	2.5	3.0	0.6
Pr_6O_{11}–MoO_3	0.83	4.2	—	0.8

[a]Weight ratio of the lanthanide oxide in the mixture (defined in Section 2.1.3).

2.3. Reaction conditions

Selective oxidation of isobutene to methacrolein was carried out in a fixed-bed U-shaped reactor system working at atmospheric pressure. The experiments were conducted with 600 mg catalyst (particle size 500–800 μm) under the following reaction conditions: molar composition of the reactant mixture (%) *i*-C_4H_8/O_2/N_2: 8.3/19.3/72.4; total flow rate: 30 ml min^{-1}, T=673 K. Gaseous reactants and products were analysed with a Di200 gas chromatograph from DELSI INSTRUMENTS. Successive measurements performed during 2 h at constant temperature indicated that the catalytic performances remained unchanged over that period of time.

2.4. Expression of the catalytical results

The catalytic performances of the various mixtures and the corresponding pure phases are listed in Tables 2 and 3, together with their mass composition (expressed as x_m (cf. Section 2.1.3) with respect to the lanthanide oxide or the lanthanide molybdate phase, col. 2), and their BET specific surface areas (col. 3). These areas were measured after submitting all the samples to the standard ultrasonic stirring described above. The results are presented in the form of isobutene conversion (X_{iso}), yield in methacrolein (Y_{met}), yield in CO_2 (expressed as $Y_{CO_2}/4$ to allow a direct comparison with isobutene conversion) and selectivity in methacrolein (S_{met}). These parameters correspond to the following definitions:

- X_{iso} is the number of mole of isobutene converted with respect to the initial number of mole of isobutene in the feed (col. 4).
- Y_{met} (or $Y_{CO_2}/4$) represents the ratio between the number of mole of methacrolein (or CO_2) formed and the number of moles of isobutene (cols. 5 and 7).
- S_{met} is defined by the ratio Y_{met}/X_{iso} (col. 6).

Columns 8–10 give the theoretical values $(X_{iso})_{th}$, $(Y_{met})_{th}$ and $(Y_{CO_2}/4)_{th}$ calculated for the various AB mixtures, supposing that the oxides do not interact and contribute to the reaction only proportionally to their amount in the mixture. This corresponds to the following expressions:

Table 2
Catalytic results obtained with the MoO_3–Pr_6O_{11} mixtures

Catalyst	x_m[a]	S_{BET}[b] ($m^2\ g^{-1}$)	X_{ISO}[c] (%)	Y_{met}[c] (%)	S_{met}[c] (%)	$Y_{CO_2}/4$[c] (%)	$(X_{ISO})_{th}$ (%)[d]	$(Y_{met})_{th}$ (%)[d]	$(Y_{CO_2}/4)_{th}$ (%)[d]
MoO_3	0	1.5	20.7	6.8	33.3	5.6	—	—	—
MoO_3/Pr_6O_{11}	0.25	2.0	18.6	4.4	23.9	5.6	21.3	5.1	7.0
MoO_3/Pr_6O_{11}	0.50	3.6	18.5	5.0	26.9	5.0	21.9	3.4	8.3
MoO_3/Pr_6O_{11}	0.75	3.2	13.1	3.9	30.1	4.2	22.6	1.7	9.7
MoO_3/Pr_6O_{11}	0.83	3.0	11.7	3.6	30.4	3.3	22.8	1.2	10.2
MoO_3/Pr_6O_{11}	0.89	3.6	14.2	2.5	17.9	4.7	22.9	0.7	10.5
Pr_6O_{11}	1	3.7	23.2	0	0	11.1	—	—	—

[a]Weight ratio of the lanthanide oxide in the mixture (defined in Section 2.1.3).
[b]Experimental specific surface area of the AB mixture.
[c]Experimental values.
[d]Theoretical values as defined in Section 2.4.

Table 3
Catalytic results: general overview

Catalyst	x_m[a]	S_{BET}[b] ($m^2\ g^{-1}$)	X_{ISO}[c] (%)	Y_{met}[c] (%)	S_{met}[c] (%)	$Y_{CO_2}/4$[c] (%)	$(X_{ISO})_{th}$ (%)[d]	$(Y_{met})_{th}$ (%)[d]	$(Y_{CO_2}/4)_{th}$ (%)[d]
MoO_3	—	1.1	13.3	5.5	41.1	2.7	—	—	—
Sb_2O_4	—	0.7	3.7	1.1	29.1	0.0	—	—	—
Pr_6O_{11}	—	2.0	20.2	0.0	0.0	9.6	—	—	—
Pr_6O_{11*}	—	3.7	23.2	0.0	0.0	11.1	—	—	—
$Pr_2Mo_3O_{12}$	—	0.6	1.4	1.4	100	0.0	—	—	—
Pr_2MoO_6	—	4.2	7.7	1.7	21.8	1.2	—	—	—
Pr_6MoO_{12}	—	7.3	29.1	0.0	0.0	13.9	—	—	—
$Pr_2Mo_3O_{12}/MoO_3$	0.50	0.7	14.1	5.8	40.8	2.7	7.3	3.4	1.3
$Pr_2Mo_3O_{12}/Sb_2O_4$	0.50	0.5	0.0	0.0	0.0	0.0	5.5	1.2	0.0
$Pr_2Mo_3O_{12}/Pr_6O_{11*}$	0.50	2.3	9.8	0.0	0.0	2.5	12.3	0.7	5.5
Pr_2MoO_6/MoO_3	0.50	2.6	21.3	6.7	31.2	5.6	10.5	3.6	1.9
Pr_2MoO_6/Sb_2O_4	0.50	2.4	3.6	1.0	29.1	0.0	8.6	1.4	0.6
Pr_2MoO_6/Pr_6O_{11*}	0.50	4.2	13.1	0.0	0.0	4.2	15.4	0.8	6.1
Pr_6MoO_{12}/MoO_3	0.50	6.2	20.1	5.7	28.1	6.6	21.2	2.7	8.3
Pr_6MoO_{12}/Sb_2O_4	0.50	5.6	13.4	0.0	0.0	4.5	19.3	0.5	6.9
Pr_6MoO_{12}/Pr_6O_{11*}	0.50	6.7	28.8	0.0	0.0	10.7	26.1	0.0	12.5
Pr_6MoO_{12}/MoO_3	0.28	3.4	15.6	7.6	48.8	7.6	17.7	4.0	5.8
Pr_6MoO_{12}/MoO_3	0.55	5.9	19.5	6.0	31.0	6.8	22.0	2.5	8.9
Pr_6MoO_{12}/MoO_3	0.85	8.0	17.2	1.7	10.0	6.5	26.7	0.8	12.2
Pr_6MoO_{12}/MoO_3	0.95	8.4	11.1	0.0	0.0	4.9	28.3	0.3	13.3
MoO_3/Pr_6O_{11}	0.44	2.0	12.0	4.9	40.8	2.8	16.3	3.1	5.7
MoO_3/Pr_6O_{11}	0.70	2.2	13.7	5.0	36.4	3.3	18.1	1.6	7.5
MoO_3/Pr_6O_{11}	0.88	2.2	9.4	2.4	25.6	2.3	19.4	0.7	8.8

[a]Weight ratio of the lanthanide oxide or molybdate phase in the mixture defined in Section 2.1.3.
[b]Experimental specific surface area of the AB mixture.
[c]Experimental values.
[d]Theoretical values as defined in Section 2.4.

$$(X_{AB})_{th} = X_A \cdot x_A + X_B \cdot x_B, \quad (1)$$

$$(Y_{AB})_{th} = Y_A \cdot x_A + Y_B \cdot x_B, \quad (2)$$

where X_i and Y_i are the experimental conversion and yield of compound i, and x_i is the weight ratio of component i in the mixture AB.

The above relationship assumes zero-order reactions as a first approximation, and isobutene conversions remaining sufficiently low so that the respective yields can be considered as proportional to the conversion values.

Apart from methacrolein (partial oxidation) and CO_2 (total oxidation), the main side products were found to be CO and formaldehyde.

Synergetic effects were investigated for the four following parameters: isobutene conversion, methacrolein yield and selectivity and CO_2 yield (Tables 4 and 5). The synergy on the different yields in AB mixtures were evaluated from the difference between the experimental values normalized for a standard specific surface area of 1 $m^2\ g^{-1}$ ($Y_{AB}/S_{BET} = Y^*_{AB}$, called real *intrinsic* yield), and the theoretical *intrinsic* yield, $(Y^*_{AB})_{th}$, i.e. the one that would be obtained in the absence of any cooperation. Because it is impossible to measure the respective surface areas developed by each phase in the mixture, the calculation of the theoretical *intrinsic* yield $(Y^*_{AB})_{th}$ was based on the following expression, in which the total surface area is evaluated from the weighted sum of the respective surface areas of the two components.

$$(Y^*_{AB})_{th} = [Y_A \cdot x_A + Y_B \cdot x_B]/[(S_{BET})_A \cdot x_A + (S_{BET})_B \cdot x_B], \quad (3)$$

where $(S_{BET})_i$ is the experimental specific surface area of compound i and x_i is the weight ratio of component i in the mixture AB.

The synergy on yield for the AB mixture, ΔY^*_{AB} was calculated according to

Table 4
Quantitative evaluation of the synergetic effects in MoO_3–Pr_6O_{11} mixtures

Catalyst	x_m[a]	$(X^*)_{th}$[b] (% g m^{-2})	$(Y^*_{met})_{th}$[b] (% g m^{-2})	$(S_{met})_{th}$[c] (%)	$(Y^*_{CO_2}/4)_{th}$[b] (% g m^{-2})	(ΔX^*_{AB}) (%)[d]	$(\Delta Y^*_{AB})_{met}$ (%)[d]	$(\Delta S_{AB})_{met}$ (%)[d]	$(\Delta Y^*_{AB})_{CO_2}$ (%)[d]
MoO_3/Pr_6O_{11}	0.25	10.4	2.5	23.9	3.3	−11	−12	0	−15
MoO_3/Pr_6O_{11}	0.50	8.4	1.3	15.5	3.2	−39	6	74	−57
MoO_3/Pr_6O_{11}	0.75	7.2	0.5	7.5	3.1	−43	126	300	−56
MoO_3/Pr_6O_{11}	0.83	6.8	0.3	5.1	3.0	−43	245	499	−63
MoO_3/Pr_6O_{11}	0.89	6.6	0.2	3.3	3.0	−41	221	449	−56

[a]Weight ratio of the lanthanide oxide in the mixture (defined in Section 2.1.3).
[b]Theoretical intrinsic values as defined in Section 2.4.
[c]Theoretical selectivity as defined in Section 2.4.
[d]Synergies as defined in Section 2.4.

Table 5
Quantitative evaluation of the synergetic effects in mechanical mixtures: general overview

Catalyst	x_m[a]	$(X^*_{ISO})_{th}$[b] (% g m^{-2})	$(Y^*_{met})_{th}$[b] (% g m^{-2})	$(S_{met})_{th}$[c] (%)	$(Y^*_{CO_2}/4)_{th}$[b] (% g m^{-2})	(ΔX^*_{AB}) (%)[d]	$(\Delta Y^*_{AB})_{met}$ (%)[d]	$(\Delta S_{AB})_{met}$ (%)[d]	$(\Delta Y^*_{AB})_{CO_2}$ (%)[d]
$Pr_2Mo_3O_{12}/MoO_3$	0.50	8.6	4.1	47.1	1.6	133	101	−13	146
$Pr_2Mo_3O_{12}/Sb_2O_4$	0.50	3.9	2.0	51.0	0.0	−100	−100	−100	0
$Pr_2Mo_3O_{12}/Pr_6O_{11*}$	0.50	5.7	0.3	5.9	2.6	−26	−100	−100	−57
Pr_2MoO_6/MoO_3	0.50	4.0	1.3	34.1	0.7	107	89	−8	195
Pr_2MoO_6/Sb_2O_4	0.50	2.3	0.6	24.4	0.2	−36	−27	19	−100
Pr_2MoO_6/Pr_6O_{11*}	0.50	3.9	0.2	5.4	1.6	−20	−100	−100	−37
Pr_6MoO_{12}/MoO_3	0.50	5.0	0.6	12.9	2.0	−36	40	117	−46
Pr_6MoO_{12}/Sb_2O_4	0.50	4.1	0.1	3.3	1.6	−41	−100	−100	−54
Pr_6MoO_{12}/Pr_6O_{11*}	0.50	4.7	0.0	0.0	2.3	−10	0	0	−28
Pr_6MoO_{12}/MoO_3	0.28	6.3	1.4	22.3	2.1	−27	58	119	8
Pr_6MoO_{12}/MoO_3	0.55	4.9	0.6	11.2	2.0	−32	86	176	−41
Pr_6MoO_{12}/MoO_3	0.85	4.2	0.1	3.1	1.9	−49	65	225	−58
Pr_6MoO_{12}/MoO_3	0.95	4.0	0.0	1.0	1.9	−67	−100	−100	−69
MoO_3/Pr_6O_{11}	0.44	11.3	2.2	19.3	4.2	−46	13	111	−66
MoO_3/Pr_6O_{11}	0.70	10.6	1.0	9.3	4.5	−41	129	292	−67
MoO_3/Pr_6O_{11}	0.88	10.3	0.4	3.5	4.7	−58	205	637	−78

[a]Weight ratio of the lanthanide oxide or molybdate phase in the mixture defined in Section 2.1.3.
[b]Theoretical intrinsic values as defined in Section 2.4.
[c]Theoretical selectivity.
[d]Synergies as defined in Section 2.4.

$$\Delta Y^*_{AB} = [Y^*_{AB} - (Y^*_{AB})_{th}]/[(Y^*_{AB})_{th}], \quad (4)$$

in which Y^*_{AB} is the real *intrinsic* yield of the AB mixture, defined as

$$Y^*_{AB} = [Y_{AB}]/[(S_{BET})_{AB}], \quad (5)$$

where $(S_{BET})_{AB}$ is the experimental specific surface area of the mixture AB and Y_{AB} is the experimental yield of the mixture AB.

In the same way, we defined the *intrinsic* isobutene conversion, $X^*_{AB} = X_{AB}/S_{BET}$, and the corresponding synergy, ΔX^*_{AB}, by the relationship

$$\Delta X^*_{AB} = [X^*_{AB} - (X^*_{AB})_{th}]/[(X^*_{AB})_{th}], \quad (6)$$

in which X^*_{AB} is the real *intrinsic* conversion of the AB mixture.

The synergy on methacrolein selectivity is defined by the following expressions:

Theoretical selectivity of AB mixture, $(S_{AB})_{th}$:

$$(S_{AB})_{th} = [Y_A \cdot x_A + Y_B \cdot x_B]/[X_A \cdot x_A + X_B \cdot x_B], \quad (7)$$

where Y_{AB} and X_{AB} are the experimental yield and conversion of the mixture AB and x_i is the weight ratio of component i in the mixture AB.

Synergy on methacrolein selectivity for the AB mixture, ΔS_{AB}:

$$\Delta S_{AB} = [S_{AB} - (S_{AB})_{th}]/[(S_{AB})_{th}]. \quad (8)$$

These values are given in the last four columns of Tables 4 and 5, for isobutene conversion (col. 7), yield in methacrolein (col. 8), selectivity in methacrolein (col. 9) and yield in CO_2 (col. 10).

3. Results and discussion

3.1. Characterization of used Pr_6O_{11}–MoO_3 catalysts

3.1.1. X-ray diffraction

As described previously [6], several praseodymium molybdate phases are detected by X-ray diffractometry in the catalysts based on the MoO_3–Pr_6O_{11} mixtures after their use in the partial oxidation reaction of isobutene. Whatever the relative amount of Pr_6O_{11} and MoO_3 engaged, the major Pr–Mo–O phase present is assumed to be Pr_6MoO_{12}, but the experimental diffraction lines are slightly shifted with respect to the corresponding powder diffraction data [9]. This phenomenon is illustrated in Fig. 1 for the sample MoO_3–Pr_6O_{11} characterized by x_m=0.89 (molar ratio Pr/Mo=6.8), which allows one to compare the experimental values (Fig. 1(a)) with the reference data (Fig. 1(b)) of the three praseodymium molybdate phases (Pr_6MoO_{12}, Pr_2MoO_6, $Pr_2Mo_3O_{12}$).

Attempts were therefore undertaken to generate the corresponding ordered phase by heating the used catalysts during 16 h in air at different temperatures. In a first series of experiments in which the used catalysts were heated in the temperature range 723–973 K, i.e. above the temperature selected for the catalytic tests, modifications are observed but cannot be easily interpreted. Moreover, at 923 K, new peaks corresponding to the Pr_2MoO_6 phase begin to appear. The results provided by a second series of experiments carried out below the reaction temperature (in the range 573–673 K) are presented in Figs. 2 and 3 which expand different 2θ-range areas (25–35° and 45–58°, respectively). In each figure, X-ray diffraction spectra are shown for the used catalyst without any thermal treatment (Fig. 2(a) and Fig. 3(a)), and after heating 16 h in air at 573 K (Fig. 2(b) and

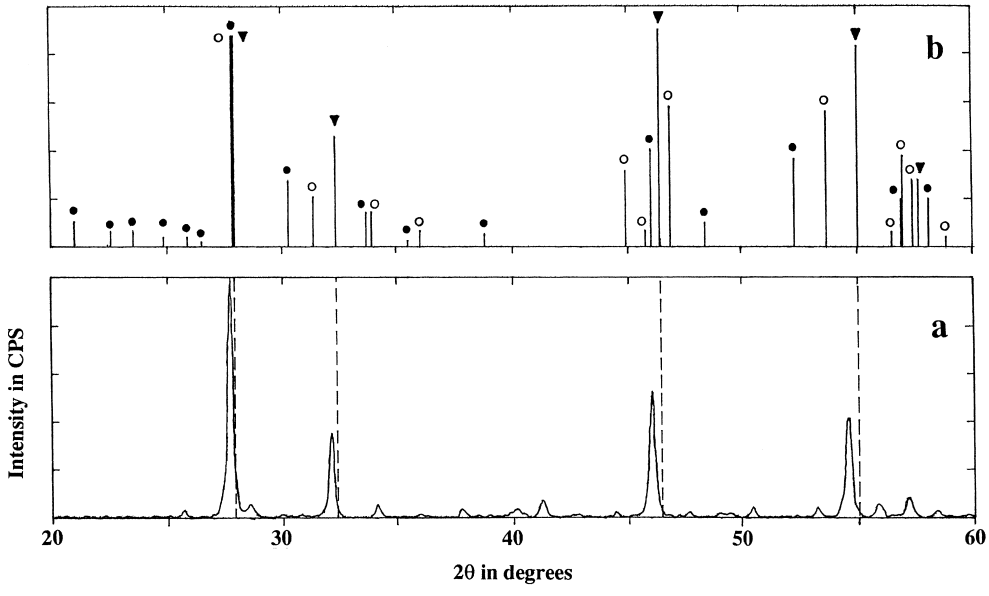

Fig. 1. (a) X-ray diffraction pattern of the used MoO_3–Pr_6O_{11} catalyst (x_m=0.89). (b) Reference powder diffraction data for Pr_6MoO_{12} (▼), $Pr_2Mo_3O_{12}$ (●), and Pr_2MoO_6 (○) [9].

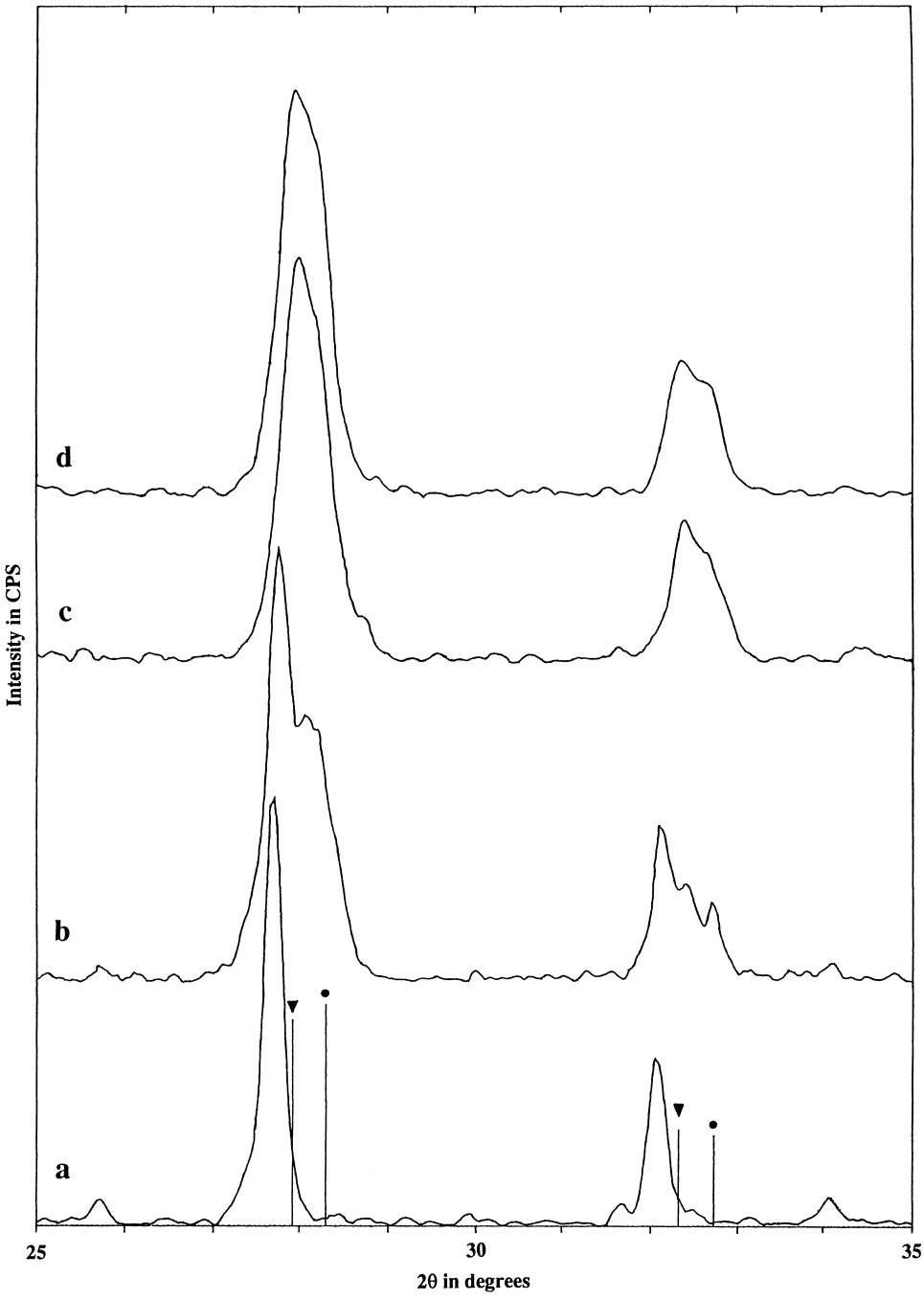

Fig. 2. X-ray diffraction pattern of the used MoO_3–Pr_6O_{11} catalyst (x_m=0.75), with reference powder diffraction data of Pr_6O_{11} (●) and Pr_6MoO_{12} (▼) [9]: (a) without any further thermal treatment; (b) after heating 16 h in air at 573 K; (c) at 623 K; (d) at 673 K.

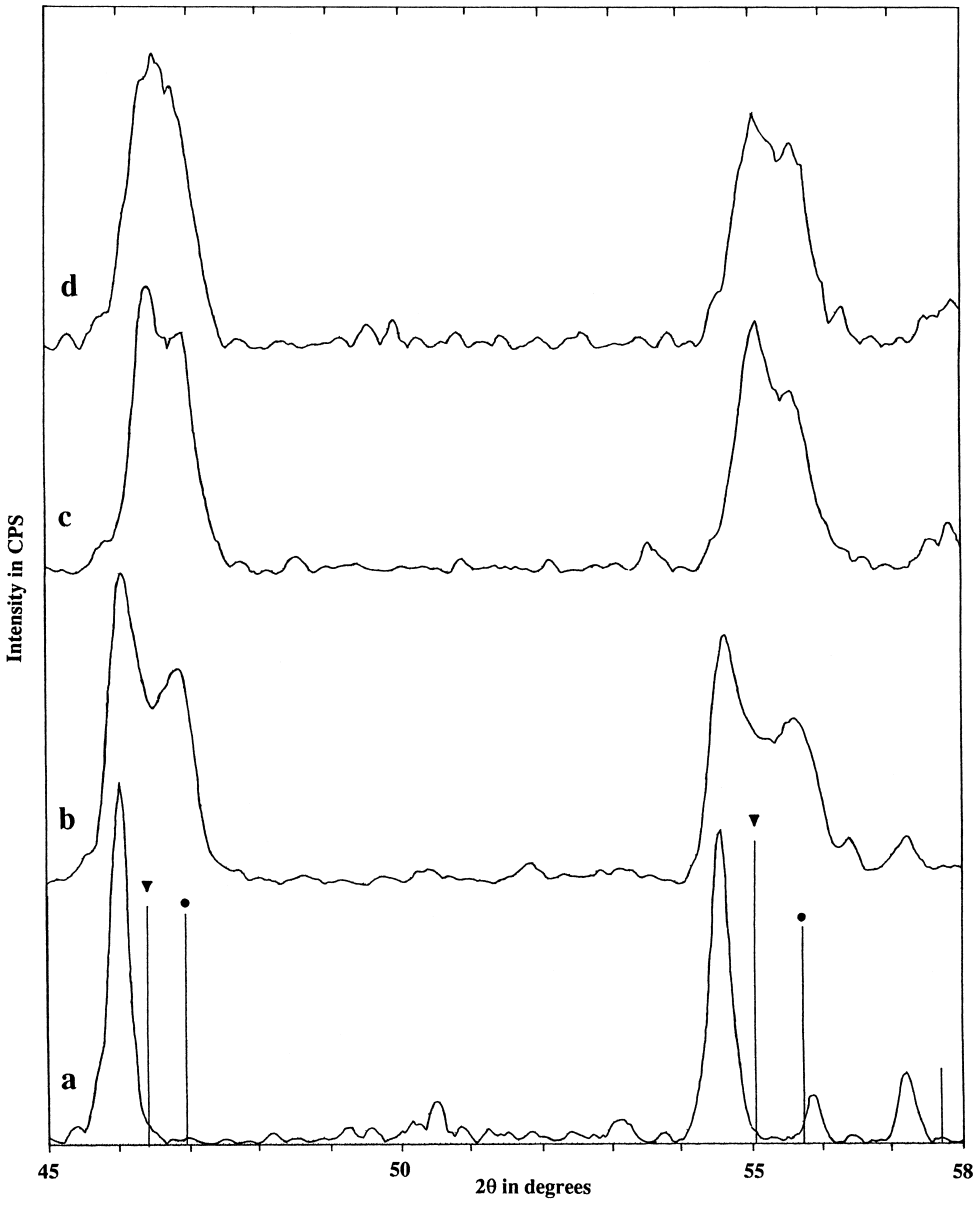

Fig. 3. Same as in Fig. 2.

Fig. 3(b)), 623 K (Fig. 2(c) and Fig. 3(c)), and 673 K (Fig. 2(d) and Fig. 3(d)). Vertical lines correspond to the powder diffraction data of the pure Pr_6O_{11} and Pr_6MoO_{12} phases.

When used catalysts are heated, the most evident features are the displacement of the four major peaks and the appearance of new components corresponding to the Pr_6MoO_{12} and Pr_6O_{11} phases (powder diffraction values). Furthermore, as the heating temperature increases, the intensity ratio between the shifted phase found after catalytic tests and the standard Pr_6MoO_{12} phase (powder diffraction data) decreases, suggesting that the first one is gradually converted into the second one. The phase detected initially in the used catalyst is

therefore assumed as corresponding to the stoichiometry Pr_6MoO_{12}, but in a disturbed environment in which the interreticular distances are larger than in the normal lattice.

3.1.2. Infrared spectroscopy

Because the literature mentions the interest of infrared spectroscopy in characterizing molybdate-type catalysts [10–17], this technique was also applied to identify the major phases present in the used catalysts. However, given the fact that the interpretation of IR results is difficult in the case of complex mixtures, the usefulness of this method is essentially related to the complementary information it provides next to more straightforward techniques like X-ray diffraction.

All our fresh and used Pr_6O_{11}–MoO_3 catalysts were submitted to an IR-analysis. Attention was focused on the 1000–400 cm^{-1} range in which the absorption bands related to the Mo–O and Ln–O–Mo stretching vibrations (Ln=lanthanide) are expected [10–12,18]. Reference IR spectra of MoO_3, Pr_6O_{11}, Pr_6MoO_{12}, $Pr_2Mo_3O_{12}$ and Pr_2MoO_6 were also recorded and are presented in Fig. 4.

3.1.2.1. Binary oxides. The IR spectrum of MoO_3 (Fig. 4(a)) is mainly characterized by a narrow line at 991 cm^{-1}, two broad bands at 867 and 607 cm^{-1}, and a rather well-defined shoulder at 820 cm^{-1}.

The spectrum of Pr_6O_{11} (Fig. 4(b)) shows essentially a narrow line at 598 cm^{-1} and a broad band below 550 cm^{-1}.

3.1.2.2. $Pr_xMo_yO_z$ phases. The three praseodymium phases exhibit IR spectra which are completely different from each other.

That of $Pr_2Mo_3O_{12}$ (Fig. 4(d)) is characterized by three well-defined peaks at 939, 916 and 420 cm^{-1}, a very broad band covering the region 900–750 cm^{-1} and another one covering the region 720–690 cm^{-1}. This IR spectrum is very similar to that of $Nd_2Mo_3O_{12}$ reported in [18]. This similarity is related to the fact that the two phases have the same scheelite-like structure [18–21] and, moreover, the effective ionic radii of Pr^{3+} and Nd^{3+} cations are very close (113 and 112.3 pm, respectively, for a coordination number of 6 [22]).

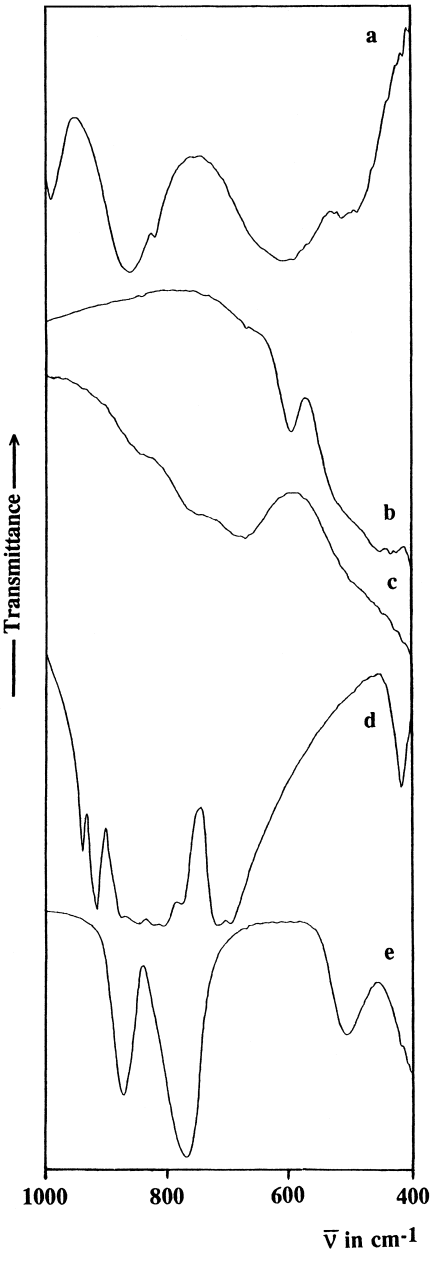

Fig. 4. Reference IR spectra of: (a) MoO_3; (b) Pr_6O_{11}; (c) Pr_6MoO_{12}; (d) $Pr_2Mo_3O_{12}$; (e) Pr_2MoO_6.

The IR spectrum of Pr_2MoO_6 (Fig. 4(e)) is characterized by three bands at 872, 769 and 509 cm^{-1}. Those values are perfectly in agreement with the literature data reported for the Ln_2MoO_6 phases (Ln=La, Pr, Nd) [23].

The spectrum of Pr_6MoO_{12} is characterized by the absence of any well-defined absorption band in that range (Fig. 4(c)).

According to studies dealing with the influence of isotopic molybdenum (^{92}Mo and ^{100}Mo) substitution in lanthanide molybdates [23,24], the wave number region 900–700 cm^{-1} corresponds to the vibrations of the MoO_4 tetrahedra and the absorption bands occurring in the range 510–340 cm^{-1} could be mainly assigned to the Ln–O bond vibrations. The fact that the Mo/Pr ratio is much weaker in Pr_6MoO_{12} than in the other two phases could therefore explain why the IR spectrum of Pr_6MoO_{12} is so elementary.

As conclusion to this section, the important point is that a comparison of the IR spectra of the three praseodymium molybdate phases shows that they are completely different; we can emphasize the use of this technique to identify which molybdate phase is present after the catalytic tests.

3.1.2.3. Mechanical mixtures of MoO_3 and Pr_6O_{11} or Pr_6MoO_{12}. Spectra of fresh and used Pr_6O_{11}–MoO_3 catalysts are presented in Figs. 5 and 6, respectively, as a function of the MoO_3/Pr_6O_{11} content (Fig. 5(a) and Fig. 6(a): x_m=0.25; Fig. 5(b) and Fig. 6(b): x_m=0.44; Fig. 5(c) and Fig. 6(c): x_m=0.70; Fig. 5(d) and Fig. 6(d): x_m=0.75; Fig. 5(e) and Fig. 6(e): x_m=0.88). Fig. 7 shows the IR spectra of several MoO_3–Pr_6MoO_{12} mechanical mixtures prepared separately to simulate the composition of the used catalysts based on the MoO_3–Pr_6O_{11} mixtures. We have to remember, as described above, that XRD suggested the presence of Pr_6MoO_{12} in these samples after the catalytic tests; however, when considering the composition of these catalysts, most of them contain an excess of MoO_3 compared to the stoichiometry of the observed product.

The comparison between the IR spectra of the fresh Pr_6O_{11}–MoO_3 mixtures (Fig. 5) and those of the corresponding pure phases (Fig. 4(a) and (b)) shows that the spectral shape changes gradually along the series as a function of the relative amount of the constituting phases. As the Pr_6O_{11} content increases in the mixture, the intensity of the bands belonging to MoO_3 at 991 and 863 cm^{-1} decreases and modifications are observed in the ranges 500–400 cm^{-1} and 700–550 cm^{-1}, with the appearance, in the Pr_6O_{11}-rich mixtures, of one peak at 596 cm^{-1}, characteristic of Pr_6O_{11}.

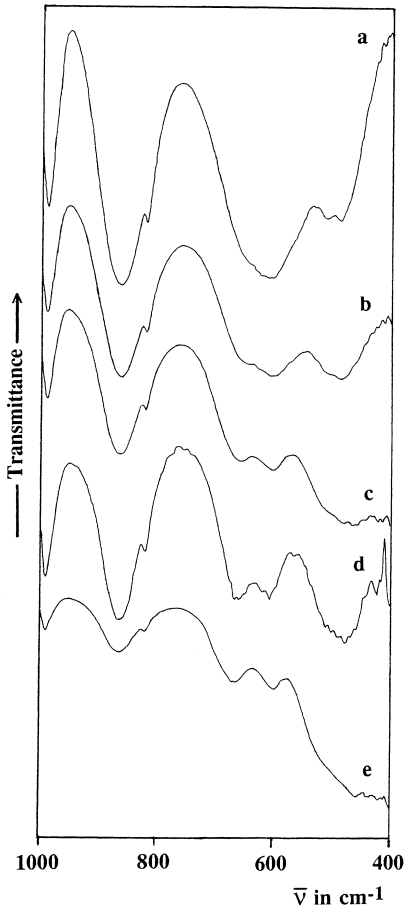

Fig. 5. IR spectra of fresh MoO_3–Pr_6O_{11} catalysts characterized by the following weight ratio: (a) x_m=0.25; (b) x_m=0.44; (c) x_m=0.70; (d) x_m=0.75; (e) x_m=0.88.

When comparing the spectra of fresh (Fig. 5) and used (Fig. 6) Pr_6O_{11}–MoO_3 catalysts, dramatic changes resulting from the catalytic process can be noted, and particularly in the Pr_6O_{11}-rich mixtures, in which a new IR band appears at 510 cm^{-1}, that can be assigned to Pr_2MoO_6.

For the MoO_3–Pr_6MoO_{12} mechanical mixtures (Fig. 7), decreasing the MoO_3 content (Fig. 7(a): x_m=0.28; (b): x_m=0.50; (c): x_m=0.85; (d): x_m=0.95) induces several major changes in the spectra: the peaks characteristic of MoO_3 in the range 1000–800 cm^{-1}, gradually vanish, together with the valley centred at above 750 cm^{-1}, whereas the valley centred at 600 cm^{-1} becomes more and more pronounced.

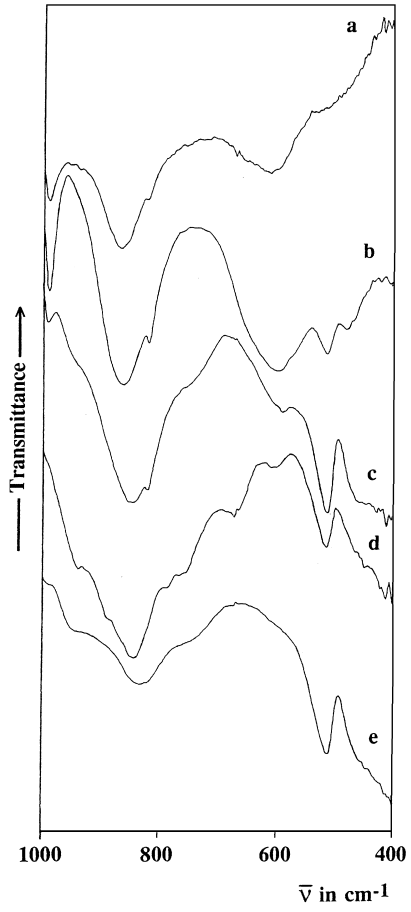

Fig. 6. IR spectra of used MoO_3–Pr_6O_{11} catalysts characterized by the following weight ratio: (a) x_m=0.25; (b) x_m=0.44; (c) x_m=0.70; (d) x_m=0.75; (e) x_m=0.88.

A few more specific comments can be formulated on the spectra obtained with the used catalysts based on the MoO_3–Pr_6O_{11} mixtures. The spectrum presented in Fig. 6(a) (x_m=0.25) resembles that of pure MoO_3 or that of a MoO_3–Pr_6MoO_{12} mixture with high molybdenum oxide content (Fig. 7(a)). The spectrum shown in Fig. 6(b) (x_m=0.44) is similar to the previous one (Fig. 6(a)) but the appearance of an additional peak at 512 cm^{-1} and the increased linewidth of the band at 862 cm^{-1} suggest the presence of small amounts of Pr_2MoO_6 (cf. Fig. 4(e)). This interpretation has been substantiated by measuring the IR spectra of MoO_3 samples in which various small amounts of Pr_2MoO_6 had been added.

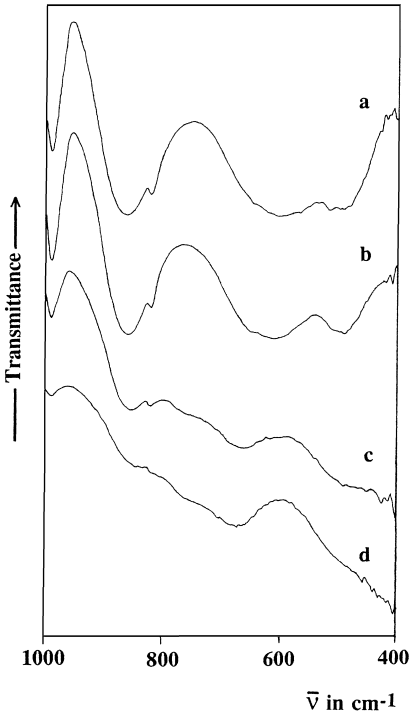

Fig. 7. IR spectra of MoO_3–Pr_6MoO_{12} mixtures characterized by the following weight ratio: (a) x_m=0.28; (b) x_m=0.50; (c) x_m=0.85; (d) x_m=0.95.

In the MoO_3–Pr_6O_{11} used mixtures, when the relative amount of Pr_6O_{11} increases (Fig. 6(e): x_m=0.88), the spectrum becomes more complex and approaches that of Pr_6MoO_{12} (Fig. 4(c)), but contains additional peaks (at 510 and 850 cm^{-1}). The absence of residual MoO_3 in this used catalyst can be deduced from the comparison with the IR spectrum of the corresponding fresh catalyst (Fig. 5(e)): the intensity of the IR bands characteristic of MoO_3 in the region 800–1000 cm^{-1} decreases and, more particularly, the band centred at 990 cm^{-1} disappears. This conclusion is furthermore in line with the shape of the IR spectrum observed for a MoO_3–Pr_6MoO_{12} mixture containing small amounts of MoO_3 (Fig. 7(d)), indicating that small amounts of MoO_3 are sufficient to generate a detectable peak at 990 cm^{-1}. As mentioned above, the more or less pronounced peak at 510 cm^{-1} is a fingerprint of Pr_2MoO_6, the presence of which also explains the perturbation in the 1000–700 cm^{-1} region. For the intermediate compositions (x_m=0.75, Fig. 6(d) and x_m=0.70, Fig. 6(c)), the IR spectra are much more

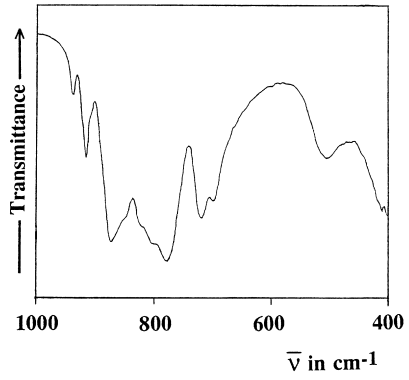

Fig. 8. IR spectra of a ternary mixture with equivalent amounts of Pr_6MoO_{12}, Pr_2MoO_6 and $Pr_2Mo_3O_{12}$.

difficult to interpret because several molybdate phases are most probably involved. This statement is in agreement with the general shape of the spectrum presented in Fig. 8, corresponding to a ternary mixture with equivalent amounts of Pr_2MoO_6, $Pr_2Mo_3O_{12}$ and Pr_6MoO_{12}, suggesting that these three praseodymium molybdate phases are probably generated together during the catalytic tests in these two samples.

3.1.3. X-ray photoelectron spectroscopy and secondary ion mass spectrometry

The surface state of some fresh and used MoO_3–Pr_6O_{11} mixtures has been characterized by XPS. The corresponding Pr/Mo intensity ratios are given in Table 1 and compared with those obtained for the three pure praseodymium molybdates (Pr_2MoO_6, $Pr_2Mo_3O_{12}$ and Pr_6MoO_{12}) and also with the theoretical Pr/Mo values related to the overall composition.

Regarding the three pure praseodymium molybdate phases, it can be noticed that experimental Pr/Mo ratios are relatively close to the theoretical ones. The same observations can be drawn for the two fresh MoO_3–Pr_6O_{11} mixtures. The low Pr/Mo values obtained for the used catalysts evidence a dramatic surface modification during the catalytic process. In two cases, this ratio is similar to the one observed for the $Pr_2Mo_3O_{12}$ phase, suggesting that $Pr_2Mo_3O_{12}$ is predominant at the surface of our used MoO_3–Pr_6O_{11} catalysts. In the third case (x_m=0.5), the high amount of MoO_3 present could be responsible for the very low value observed, if one takes into account the analysis depth of the XPS technique and the fact that in this sample, MoO_3 is in excess with respect to the formation of the two detected praseodymium molybdates (bulk molar ratio Pr/Mo=0.8, compared to Pr_6MoO_{12} in the bulk, $Pr_2Mo_3O_{12}$ at the surface).

In order to provide a deeper insight into the differences between the surface and bulk compositions of our used catalysts, the samples were also characterized by static time-of-flight secondary ion mass spectrometry (ToF SIMS). In comparison with XPS, only the outermost atomic layers are analysed. In addition, the SIMS technique gives access to molecular information. The experimental results collected with the fresh and used MoO_3–Pr_6O_{11} mixtures have been described extensively elsewhere [7]. In that work, ToF SIMS has been shown to be a very powerful technique for discriminating between the three praseodymium molybdates. This was due to the fact that $Pr_2Mo_3O_{12}$ and Pr_6MoO_{12} possess characteristic ToF SIMS high-mass fragments, and also because linear relationships were found between the intensity ratios of several fragments and the molar bulk composition of the three pure molybdate phases. The main conclusions concerning the used MoO_3–Pr_6O_{11} catalysts were that (1) despite the fact that this phase was predominant in the bulk, no Pr_6MoO_{12} molybdate was found at the surface; (2) ToF SIMS unequivocally validated the XPS results by confirming that $Pr_2Mo_3O_{12}$ was the major phase at the surface of these used catalysts.

3.2. Catalytic results

To make the interpretation of the catalytic results easier, Tables 2 and 4 summarize the experimental data previously obtained for the MoO_3–Pr_6O_{11} mixtures. These results have been discussed in detail elsewhere [6] and summarized in the above introduction.

The experimental data obtained within the frame of the present work are listed in Tables 3 and 5.

3.2.1. Pure $Pr_xMo_yO_z$ phases

The catalytic performances of the three pure praseodymium molybdates (*intrinsic* values, as defined in Section 2.4.) are listed in Table 3. It appears that (i) $Pr_2Mo_3O_{12}$ is active for partial oxidation only and produces no CO_2 at all, (ii) Pr_6MoO_{12} displays an overall higher activity but does not produce any

methacrolein, being active for total oxidation only, and (iii) Pr_2MoO_6 exhibits an intermediate behaviour with a moderate activity towards partial and total oxidation. However, when these data are normalized with respect to the respective specific surface areas (*intrinsic* values given in col. 3 of Table 3), the isobutene conversions are found to be 2.3, 1.8 and 3.9% g m^{-2}, for $Pr_2Mo_3O_{12}$, Pr_6MoO_{12} and Pr_2MoO_6, respectively, showing that the larger activity of the Pr-rich phase essentially reflects its higher division state. The main observation remains here that the pure $Pr_2Mo_3O_{12}$ and Pr_2MoO_6 display a completely different behaviour with respect to isobutene oxidation.

3.2.2. $Pr_xMo_yO_z$ phases mixed with Sb_2O_4

When mixed with Sb_2O_4, the three molybdate phases give rise to a negative synergy on the conversion rate, which becomes zero in the case of the mixture with $Pr_2Mo_3O_{12}$. Negative synergetic effects also appear on methacrolein production (Table 5, col. 8), and are more pronounced in the case of Pr_6MoO_{12} and $Pr_2Mo_3O_{12}$. Except for $Pr_2Mo_3O_{12}$, there is also a negative synergy on CO_2 production (Table 5, col. 10).

3.2.3. $Pr_xMo_yO_z$ phases mixed with MoO_3

The results obtained for the $Pr_xMo_yO_z$–MoO_3 mechanical mixtures (Table 5) are more dissimilar and can be summarized as follows, plus (+) and minus (−) signs referring to positive and negative synergy, respectively.

Molybdate phase mixed with MoO_3	Synergy on conversion rate	Synergy on methacrolein yield	Synergy on CO_2 yield
$Pr_2Mo_3O_{12}$	+	+	+
Pr_6MoO_{12}	−	+	−
Pr_2MoO_6	+	+	+

It appears that only the Pr_6MoO_{12}–MoO_3 mixtures exhibit the same general tendencies as the MoO_3–Pr_6O_{11} catalysts, i.e. negative synergy on isobutene conversion rate, positive synergetic effects on the methacrolein yield and decrease of total oxidation. For this reason, the Pr_6MoO_{12}–MoO_3 mixtures were considered as ideal candidates for deeper investigations.

A special comment must be made concerning the Pr_6MoO_{12}–MoO_3 mixture which is the richest with respect to Pr, namely that corresponding to x_m=0.95. In that case, clear negative synergetic effects occur on all investigated parameters. This mixture displays a catalytic behaviour very similar to that of pure Pr_6MoO_{12}. Considering the significant difference between the specific surface areas of these phases, this could be explained by the fact that the small particles of Pr_6MoO_{12} are coating the larger MoO_3 particles, thus suppressing the beneficial effect of MoO_3 on yield.

3.2.4. $Pr_xMo_yO_z$ phases mixed with Pr_6O_{11}

In all the mixtures based on Pr_6O_{11}, methacrolein production is totally inhibited and the CO_2 yields reflect merely the cumulative contributions of each pure phase. These results allow to conclude that the positive cooperation observed for partial oxidation in the Pr_6O_{11}–MoO_3 mixtures [6] cannot be directly assigned to synergetic effects between the different $Pr_xMo_yO_z$ phases generated in these catalysts during their operation and the eventual excess of Pr_6O_{11}.

3.2.5. Stability of the catalysts under the reaction conditions

To investigate the stability of the catalysts under the reaction conditions, all the used catalysts were analysed by X-ray diffractometry. Complementary experiments were however carried out outside the catalytic reactor to measure the intrinsic thermal stability of these catalysts and look at the eventual occurrence of solid state reactions, by submitting all the fresh samples to heating during 16 h in air at 673 and 773 K.

Concerning the used catalysts, the three pure praseodymium molybdate phases and all their mixtures with MoO_3, Sb_2O_4 or Pr_6O_{11} were found to be stable under the reaction conditions. In particular, the metastable Pr_6MoO_{12} phase, reported previously as generated in the Pr_6O_{11}–MoO_3 mixtures, has never been found. Whereas thermal treatments during 16 h in air at 673 K were shown to cause no modifications in the above-mentioned mixtures, new solid crystalline phases were observed in the $Pr_xMo_yO_z$–MoO_3 mix-

tures heated at 773 K. The identification of the phases present in these samples is very difficult and the coexistence of several praseodymium molybdate phases is generally suspected. It seems worth reminding that ternary $Pr_xMo_yO_z$ phases were already known to be generated in Pr_6O_{11}–MoO_3 mixtures heated at 773 K [6].

3.3. Discussion

Before formulating comments or assumptions when comparing the catalytic properties of some samples, we have to keep in mind that bulk praseodymium molybdates and the ones generated in situ might show different catalytic behaviours. Nevertheless, the comparison seems to be useful for a better understanding of the present experimental results.

3.3.1. Role of the $Pr_2Mo_3O_{12}$ phase

The presence of the $Pr_2Mo_3O_{12}$ phase, identified by XPS and ToF SIMS as being the major one at the surface of the used MoO_3–Pr_6O_{11} catalysts, does not seem to account for the observed synergetic effects (i.e. negative synergy on isobutene conversion rate, positive synergetic effects on the methacrolein yield and decrease of total oxidation). As a pure phase, the $Pr_2Mo_3O_{12}$ molybdate is almost inactive. In the mixture with MoO_3, isobutene conversion, methacrolein yield and CO_2 yield are globally enhanced. In the mixture with Pr_6O_{11}, there is a negative synergy on methacrolein selectivity.

3.3.2. Comparison between $Pr_xMo_yO_z$ phases and MoO_3–Pr_6O_{11} mechanical mixtures

The last three lines of Tables 3 and 5 refer to MoO_3–Pr_6O_{11} mechanical mixtures displaying the same Pr/Mo molar composition as the three pure praseodymium molybdate phases, i.e. x_m=0.44 for $Pr_2Mo_3O_{12}$, x_m=0.70 for Pr_2MoO_6 and x_m=0.88 for Pr_6MoO_{12}. As far as conversion is concerned (Table 3, col. 5), it appears that the MoO_3–Pr_6O_{11} mixtures are always more active than the pure praseodymium molybdate phase having the same Pr/Mo composition. The same tendency appears when the methacrolein production is considered (Table 3, col. 5); more particularly, the mixture characterized by x_m=0.88 is active for partial oxidation while the corresponding Pr_6MoO_{12} phase did not produce methacrolein. The MoO_3–Pr_6O_{11} mixtures are also more selective than the corresponding molybdate phases except for $Pr_2Mo_3O_{12}$, which is very selective for methacrolein (Table 3, col. 6). CO_2 production is generally enhanced in the mixtures (Table 3, col. 7), except for x_m=0.88, because Pr_6MoO_{12} was shown to produce CO_2 exclusively.

3.3.3. Comparison between MoO_3–Pr_6O_{11} and MoO_3–Pr_6MoO_{12} mixtures

Because Pr_6MoO_{12} is the predominant bulk phase detected by X-ray diffraction and is furthermore the only phase that displays the same general catalytic behaviour, when mixed with MoO_3, as the one observed in the MoO_3–Pr_6O_{11} mixtures, the influence of the Pr–Mo composition on the catalytic behaviour has been investigated with greater care. In order to determine if the catalytic behaviour of the previously investigated MoO_3–Pr_6O_{11} mixtures [6] is due to cooperation phenomena between separate phases or has to be assigned to the generation of molybdate phases, additional MoO_3–Pr_6MoO_{12} mixtures characterized by the same Pr/Mo molar ratio as the MoO_3–Pr_6O_{11} mixtures studied before were synthesized and tested for their catalytic performances (x_m=0.28; 0.55; 0.85; 0.95). A comparison between these MoO_3–Pr_6MoO_{12} mixtures (Tables 3 and 5) and MoO_3–Pr_6O_{11} mixtures (Tables 2 and 4) is presented in Fig. 9, which shows the evolution of the synergies on methacrolein yields and selectivities as a function of the Pr/Mo molar ratio. For mixtures with Pr_6MoO_{12}, as the Pr/Mo ratio increases, a general decrease of these quantities is noticed. These observations are completely different from those noted in the MoO_3–Pr_6O_{11} mixtures. Moreover, considering the MoO_3–Pr_6O_{11} composition that gives rise to the more pronounced cooperation effects (x_m=0.83), the corresponding MoO_3–Pr_6MoO_{12} mixture does not produce any methacrolein. It seems therefore that the synergetic effects observed in the MoO_3–Pr_6O_{11} mixtures cannot be explained by the generation of Pr_6MoO_{12} during the tests.

4. Conclusions

The purpose of the present work was, first, to identify the major $Pr_xMo_yO_z$ phase generated under

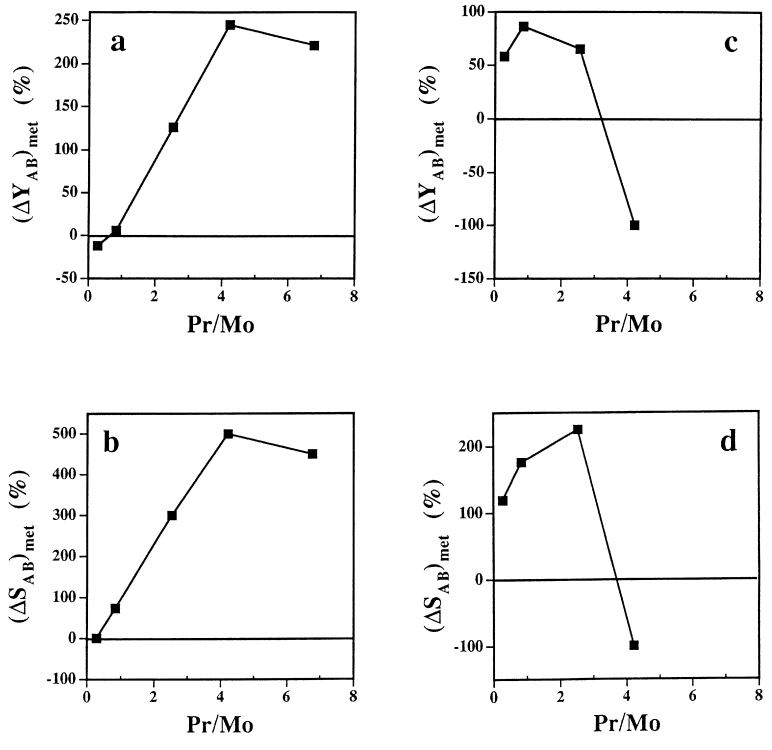

Fig. 9. Synergy on yield (a, c) and selectivity (b, d) in methacrolein as a function of the Pr/Mo molar ratio for Pr_6O_{11}–MoO_3 (a, b) and Pr_6MoO_{12}–MoO_3 (c, d) mixtures.

the reaction conditions when MoO_3–Pr_6O_{11} mixtures were used for the isobutene-to-methacrolein conversion. The composition of the used catalysts is very complex. As indicated mainly by X-ray diffraction but also by IR data, a metastable Pr_6MoO_{12} phase is always present and is the major molybdate in the bulk. Time-of-flight secondary ion mass spectrometry and X-ray photoelectron spectroscopy also show that $Pr_2Mo_3O_{12}$ is dominant at the surface.

The second objective was to investigate whether the catalytic behaviour of these catalysts could be explained by the intrinsic catalytic properties of the various ternary $Pr_xMo_yO_z$ phases spontaneously generated in situ, or by a cooperation between separate phases (ternary $Pr_xMo_yO_z$ phases and/or unreacted binary oxides, MoO_3 or Pr_6O_{11}).

A major conclusion is that the cooperative effects previously observed in the MoO_3–Pr_6O_{11} mixtures cannot be attributed exclusively to the intrinsic catalytic properties of praseodymium molybdates. A cooperation is also observed between couples of oxide phases: Pr_6MoO_{12} displays donor properties with respect to MoO_3. The evolution of the catalytic properties of Pr_6MoO_{12}–MoO_3 mixtures with respect to the Pr/Mo content is completely different from the one observed in MoO_3–Pr_6O_{11} mixtures. It does not seem that the observed synergetic effects could be assigned to the simultaneous presence of ternary $Pr_xMo_yO_z$ phases and Pr_6O_{11}.

The generation of praseodymium molybdate phases during the catalytic tests seems therefore to play no significant role in the catalytic behaviour of MoO_3–Pr_6O_{11} mixtures. Owing to the complexity of the composition of our used MoO_3–Pr_6O_{11} catalysts and to the fact that the catalytic properties of bulk synthesized praseodymium molybdates and in situ generated ones might be different, the rationalization of the present results in the framework of the remote control theory is therefore by far not obvious.

Acknowledgements

The authors greatly acknowledge financial support from the Belgian National Fund for Scientific Research (FNRS, Brussels).

References

[1] L.T. Weng, B. Delmon, Appl. Catal. A 81 (1992) 141.
[2] L.T. Weng, S.Y. Ma, P. Ruiz, B. Delmon, J. Mol. Catal. 61 (1990) 99.
[3] P. Ruiz, B. Zhou, M. Remy, T. Machev, F. Aoun, B. Doumain, B. Delmon, Catal. Today 1 (1987) 181.
[4] L.T. Weng, P. Ruiz, B. Delmon, J. Mol. Catal. 52 (1989) 349.
[5] L.T. Weng, P. Ruiz, B. Delmon, Stud. Surf. Sci. Catal. 72 (1992) 399.
[6] F. De Smet, P. Ruiz, B. Delmon, M. Devillers, Catal. Lett. 41 (1996) 203.
[7] F. De Smet, M. Devillers, C. Poleunis, P. Bertrand, J. Chem. Soc., Faraday Trans., 94 (1998) 941.
[8] C. Marcilly, Ph. Courty, B. Delmon, J. Am. Ceram. Soc. 53 (1970) 56.
[9] Powder diffraction data, J.C.P.D.S.-I.C.D.D.: Pr_6MoO_{12} (24-1116), $Pr_2Mo_3O_{12}$ (24-0911) and Pr_2MoO_6 (24-0913).
[10] M. Devillers, F. De Smet, O. Tirions, Thermochim. Acta 260 (1995) 165.
[11] J.H.G. Bode, H.R. Kuijt, M.A.J.Th. Lahey, G. Blasse, J. Solid State Chem. 8 (1973) 114.
[12] M.J. Schwing-Weill, Bull. Soc. Chim. France 5 (1972) 1754.
[13] I. Matsuura, R. Schuit, K. Hirakawa, J. Catal. 63 (1980) 152.
[14] S. Bhat, P.N. Kotru, J. Mater. Sci. 30 (1995) 2694.
[15] F. Shi, J. Meng, Y. Ren, J. Solid State Chem. 121 (1996) 236.
[16] M.R. Sun-Kou, S. Mendioroz, J.L.G. Fierro, J.M. Palacios, A. Guerrero-Ruiz, J. Mater. Sci. 30 (1995) 496.
[17] M.S. Augsburger, J.C. Pedregosa, J. Phys. Chem. Solids 56 (1995) 1081.
[18] M. Del, C. Viola, A.M. Sangra, J.C. Pedregosa, J. Mater. Sci. 28 (1993) 6587.
[19] W. Jeitschko, Acta Cryst. B 29 (1973) 2074.
[20] L.H. Brixner, Rev. Chim. Minér. 10 (1973) 47.
[21] J. Gopalakrishnan, A. Manthiram, J. Chem. Soc., Dalton Trans. (1981) 668.
[22] R.D. Shannon, Acta Cryst. A 32 (1976) 751.
[23] V.V. Fomichev, O.I. Kondratov, V.A. Gagarina, L.Z. Gokhman, K.I. Petrov, Russ. J. Inorg. Chem. 22 (1977) 1163.
[24] V.V. Fomichev, V.A. Gagarina, O.I. Kondratov, L.A. Gribov, K.I. Petrov, Russ. J. Inorg. Chem. 26 (1981) 958.